Chemical and kinematic analysis of the ancient star J0449−5656 and its origins in the early universe

Jiayi(Jennifer) Zhou

September 2022

Abstract

In this study, I researched an ancient metal-poor star based on a high-resolution spectrum taken with the 6.5 m Magellan Telescope in Chile. I determined the radial velocity of the star of 110 km/s. I then measured equivalent widths of many absorption lines in the spectrum to determine the chemical abundances of light, iron-peak and heavy elements. I also did a kinematic analysis of the star's orbital motion over the last 10 billion years. My findings are as follows: J0449−5656 is an ancient halo star that formed from gas enriched by a massive 20 solar mass progenitor energetic hypernova explosion as well as a neutron-star-merger that created the heavy elements, such as europium, which is found in large amounts in J0449−5656. The star likely formed in an early dwarf galaxy, which was accreted by the Milky Way galaxy a long time ago. This explains how J0449−5656 entered the halo where it has resided since.

1 Introduction

13.8 billion years ago, the universe started with the Big Bang in a massive explosive event. Ever since then, it has continued expanding and will continue to do so at an even fast pace going forward. Hydrogen, helium and lithium were the only three elements present in the very early universe. The heavier elements up to iron were first formed through the process of nuclear fusion within stars once the first stars had formed. These very first stars were very massive, around 100 solar masses, because the early H, He and Li gas was not able to cool well, clump, and make small stars. This cooling problem would only change later once other elements had been added to the gas. Then numerous generations of stars were able to form, including low-mass stars such as the Sun [6].

The successive build up of the heavier elements in the universe over time is called chemical evolution. This process describes the overall composition of the universe as it changes with time and place. Due to the process of chemical evolution, the amount of heavy elements increases with time, a trend that continues today. Therefore, stars born early in the universe contain less of all the heavy elements than stars born more recently, such as the Sun (it was born 4.6 billion years ago). These early stars were mainly formed from hydrogen and helium, with just a tiny amount of heavier material [4, 5].

Oddly, in astronomy, metals are referred as elements that are heavier than hydrogen and helium, which essentially are all the elements that are formed in nuclear fusion within stars, as well as other processes operating in other sites. Astronomers thus call stars formed early on in the universe "metal-poor stars," in reference to their small amount of heavy elements compared to the Sun. Metal-poor stars are some 13 billion years old. [4, 6] Accordingly, they allow astronomers to carry out research in the field called "stellar archaeology," which explores the early universe with the oldest stars. The chemical abundance patterns of the heavy elements observed in these ancient stars provide details to the origin of chemical elements and how they formed from nucleosynthesis processes occurring in the cores of stars, the supernova explosions of different types of massive stars and neutron star mergers. In fact, all the elements observed in old stars today were not made by the stars themselves, which are still burning hydrogen to helium for billions of years and will do so several additional billions of years. Therefore, the observed elements were formed prior to the old stars' births in the early universe, e.g. the first supernova explosions that ever occurred. Old stars simply preserve the "nucleosynthetic fingerprints" of these early nucleosynthesis events. Studying old stars

also provides information on the formation processes of the earliest generations of stars and the very first galaxies a few hundred million years after the Big Bang. This is the basic concept of stellar archaeology. [4, 6]

This stellar archaeology approach is complementary to other techniques used to study the early universe. For example, in order to observe the most distant galaxies at very high redshift that were born soon after the Big Bang, their light must have travelled for billions of years. These observations show the galaxies at their earliest phase of evolution, around 12 to 13 billion years ago, which allows astronomers to learn about the process of galaxy formation back then [5].

Some of the oldest stars discovered about believed to be 13 billion years old and of the second generation of stars in the universe. Two examples are HE1327−2327 and HE0107−5240 [7], two stars that have recorded low abundances of iron, which suggests that only one previous supernova explosion could have produced the now-observed elements in these stars. Another example is BD+44 493 [9], which is also thought to be a second generation star that is very bright and easy to observe. Its chemical composition includes an overall low iron abundance together with a high carbon-to-iron ratio. This signature has also been found in the other two stars. In the ultraviolet spectrum of BD +44 493, astronomers discovered phosphorus, sulfur, and (most importantly) zinc, which had been only observed once in second generation stars. Zinc is important as it provides information on the explosion energy of the progenitor star that made the now-observed elements.

Stellar archaeology is a very exciting field as it provides valuable information about the beginning of star and galaxy formation. However, a main difficulty in making further progress is a lack of the most metal-poor stars. The oldest stars from the second or earliest few generations are extremely rare and sprinkled all over our Milky Way galaxy. This means that they are hard to find, and often very faint, which makes observations difficult to make and limits the measurements astronomers can take. Therefore, and example of a consequence is that there remains too little evidence on the variety of chemical abundance pattern and their frequencies of occurrence to complete our understanding of the theory of early stars and early galaxies formation. This problem also limits our knowledge on how heavy elements were formed in the first stars for the first time.

This project is an analysis of the element abundance signature of the metal-poor star J0449−5656, together with a kinematic analysis that shows how the star has been moving about the galaxy for billions of years. Altogether, this tells information about its formation location and history.

2 Observations and Measurements

2.1 Telescope observations

J0449−5656 was selected as part of an ongoing program to find the most metal-poor stars by Prof.Frebel, who has been searching for these oldest objects for two decades. Sky surveys, such as RAVE, were used to select candidates. Verification of candidates happened with large telescopes, such as the Magellan telescope in Chile. Stars that look promising would then be observed again for better data.

We observed J0449−5656 with coordinate right ascension R.A. = 04:49:17.8, and declination decl. = −56:56:08.5 (J2000.0) with the MIKE spectrograph [2] on the 6.5 meter Magellan-Clay telescope at Las Campanas Observatory on 2020 December 18. To capture the observations, a 07 slit was used, which yields a high spectral resolution of 28,000 in the red and 35,000 in the blue wavelength regime of the spectrum. The total exposure time was 3 hr, although the seeing degraded during the second half of the observations.

The data quality is quite high, as the resulting signal-to-noise ratio per pixel is 144 at 5990Å. This makes for a relatively smooth spectrum with absorption lines easy to measure. Below several portions of the spectrum are shown.

2.2 Radial Velocity Measurements

In astronomy, the measurement of a celestial object's speed and moving direction along the line of sight is called the radial velocity. It can be measured by the location of absorption lines in a stellar spectrum. Due to the star's motion in space, the wavelengths of the lines in the spectrum shift relative to the rest frame. This movement is a reflection of the Doppler Effect.

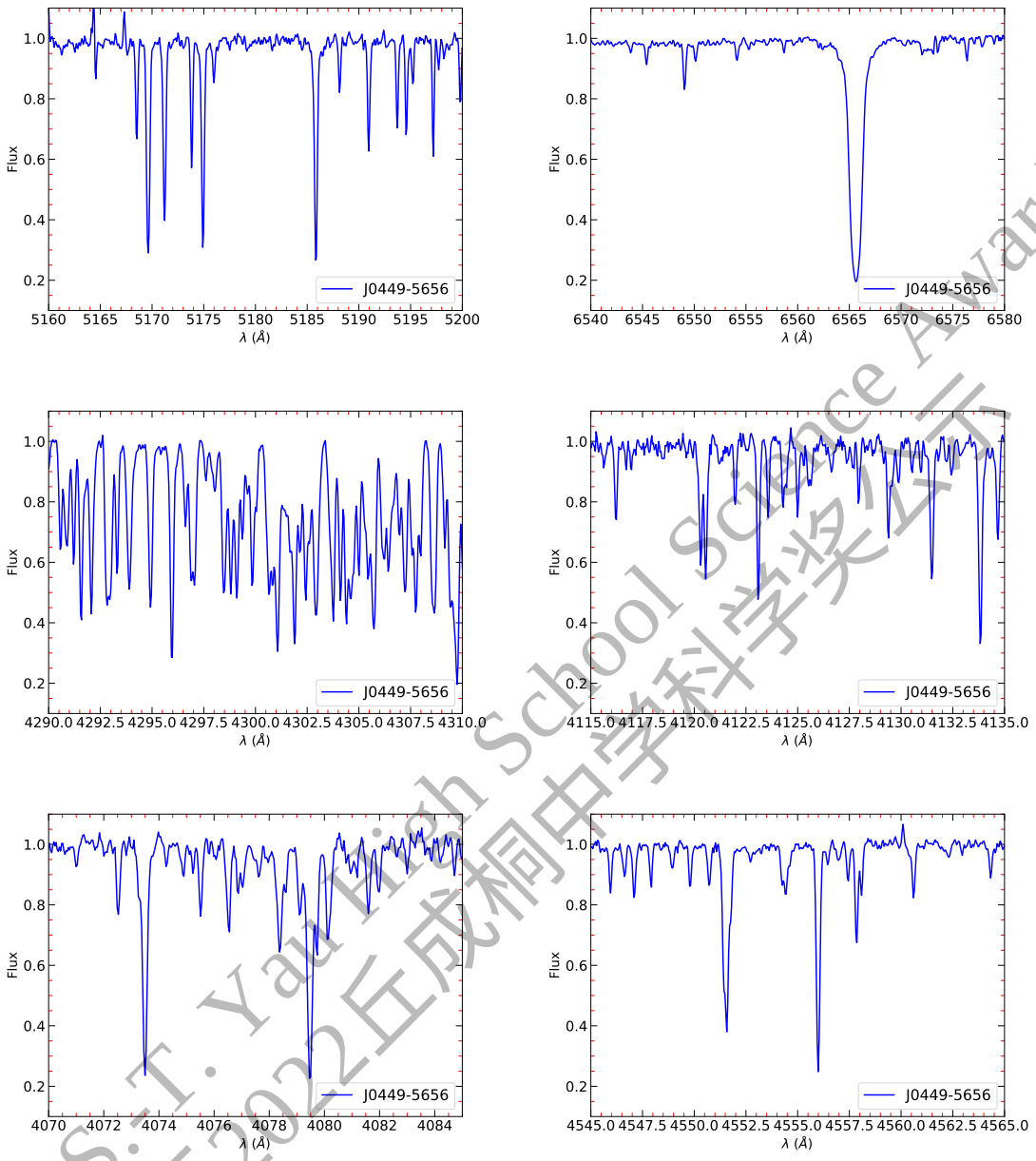

Figure 1: Portions of the spectrum of J0449−5656, around the Mg b lines at 5180 Å, around the H line at 6562 Å, around the Eu line at 4129 Å, around Sr line at 4077 Å and 4554 Å

One method to determine the radial velocity of a celestial object is by plotting a graph with two spectra: one of the target star and the other one being a comparison star with a spectrum shifted to rest. I then measured the wavelength of the core of the Hα line, first by eye and then with a ruler. Once the wavelengths of both lines were found, the velocity can be calculated from the difference $\Delta\lambda$, the known wavelength of the line λ, and the constant for the speed of light, i.e. $\Delta\lambda/\lambda = v/c$.

The uncorrected spectrum of J0449−5656 (blue line) and the rest frame spectrum of HD140283 (red line; another metal-poor star) are shown in Figure 2.

The second method is used with computers, called "cross correlation," which mathematically compares the stellar spectrum with a template spectrum that has a recorded velocity. It searches for a overlap match

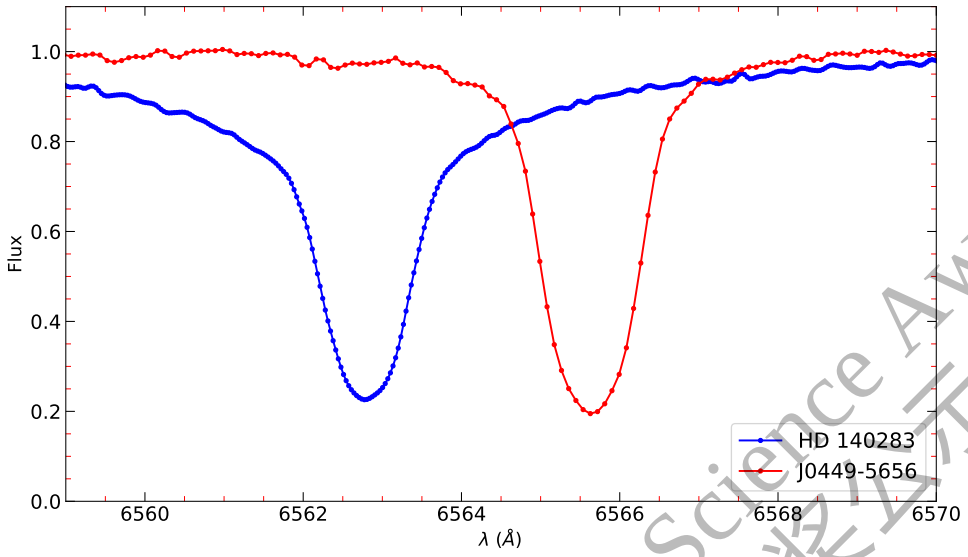

Figure 2: Portion of the spectrum around H_α line of the target star J0449−5656 compared to that of our comparison star HD140283. J0449−5656 has not been radial velocity corrected, so its spectrum is not at rest yet.

of the two spectrum. The radial velocity can then be determined; it is the peak of the cross-correlation graph.

Both methods gave a geocentric radial velocity, which is a measurement taken relative to Earth instead of the Sun. Therefore, to find the heliocentric radial velocity, the heliocentric correction needs to be added to the geocentric radial velocity. The heliocentric correction can be calculated with existing astronomy computer programs.

When the final heliocentric radio velocity is negative, it means that the object is moving towards the observer because the measured absorption line was blue-shifted (had shorter wavelengths) compared to the line in the template spectrum. Oppositely, a positive radial velocity suggests that the object is moving away from the observer; its lines were red-shifted (appeared at longer wavelength). The results for the geocentric radial velocity were +128.8 km/s from the first methods and +125 km/s from the second method. I calculated −18.43 km/s as the heliocentric correction. Adding it to the geocentric correction gives +110.37 km/s (using the second method).

2.3 Equivalent Width Measurements

The measurement of the strength of the absorption lines in a spectrum is the equivalent width, which is calculated by the area under the curve of each absorption line. Every element has its own absorption lines, and every measured line will be used to calculate its abundance. An essential part in calculating the equivalent width is identifying if the correct absorption line if measured and whether the program provided a good line or not.

I used an automated program called pyEW (https://github.com/madamow/pyEW) to measure equivalent widths. Figure 3 shows examples of four measured Fe I lines. In total, about 400 absorption lines were measured of various elements across the entire spectrum between about 3500 Å and 6500 Å. When both the Gauss and the multi-Gauss fit matched the continuum and the spectrum nicely without any point on the continuum missing, then the respective line measurement was kept for the chemical abundance determination. If there was a small mismatching on parts of the fitted function, then I slightly adjusted the equivalent width depending on the amount of the spectrum that did not match the fit well. Well-fit lines are those in the top

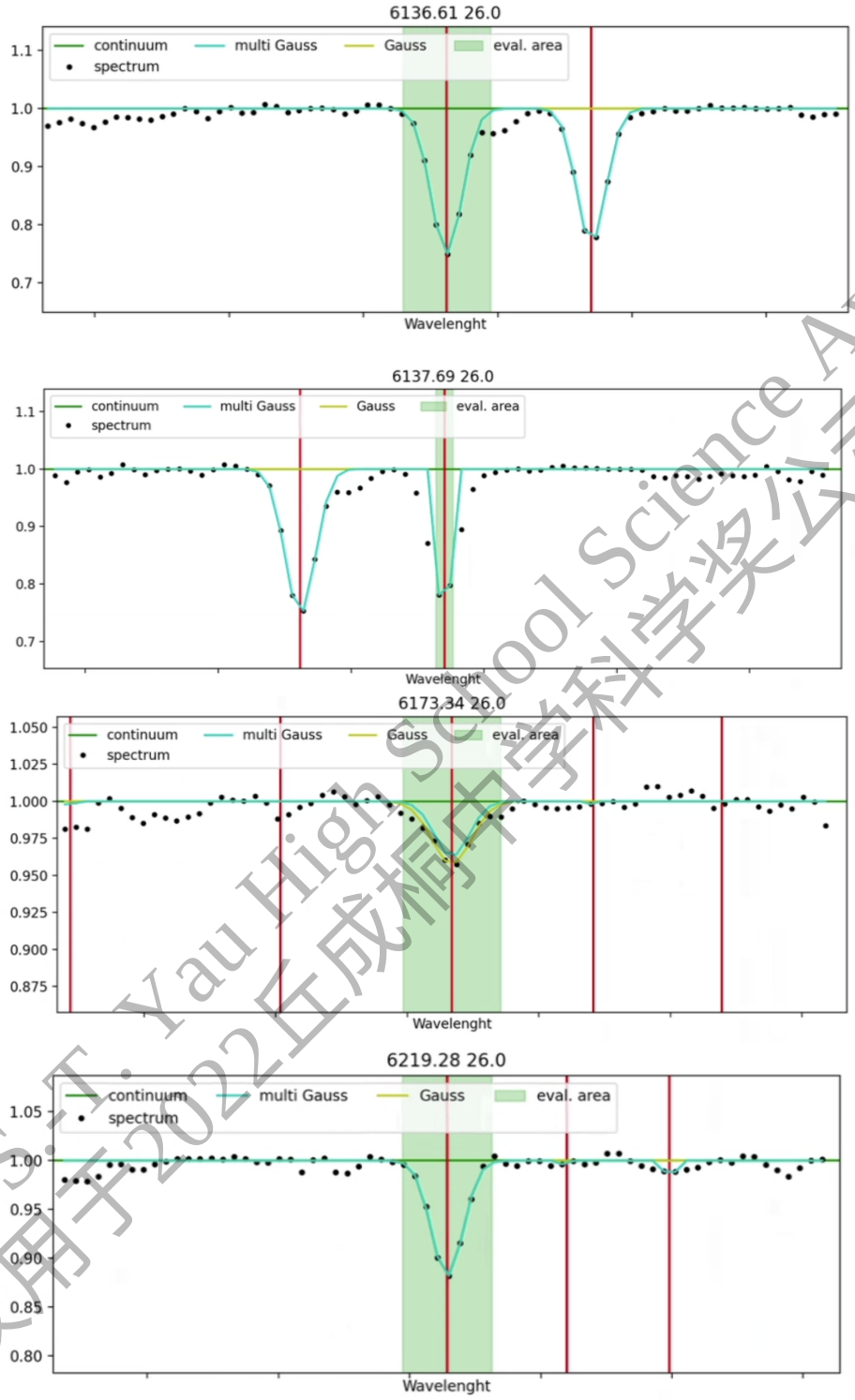

Figure 3: Top panel: Fe I line with good multi-Gauss fit. Second panel: Fe I line that is problematic. Third panel: Fe I line with Gauss and multi-Gauss mismatch. Bottom panel: Fe I line with good multi-Gauss fit.

and bottom panels of Figure 3.

In the case that the Gauss and multi-Gauss fits gave different values, I chose the equivalent width that matched the spectrum and the continuum better. Then this value was used for the abundance measurement. An example is shown in the third panel from the top in the figure. The multi-Gauss fit does not match the data well (small black dots); instead I chose the equivalent width from the Gauss fit. Finally, when the continuum, spectrum, Gauss and multi-Gauss fits are completely not matching, the problematic line would be noted down and later discarded from further measurements. An example can be seen in the second plot from the top in the Figure.

3 Chemical Abundance Analysis

3.1 Stellar Parameters

Stellar parameters are the effective temperature, T_{eff}, at the surface of the star, the surface gravity (log g), the overall element abundance, metallicity (as given by the iron abundance, [Fe/H]), as well as the micro-turbulence which is needed for running the model atmosphere analysis to obtain the chemical abundances. They describe the physical properties of the absorption happens in the star.

Determining stellar parameters is a challenging process that requires a lot of different information. Due to this reason, it was not a direct part of this project but stellar parameters are necessary for the chemical abundance analysis. Prof.Frebel provided the stellar parameters for my star. The metallicity was based on my equivalent width measurements of ∼200 Fe lines, though. The values are $T_{eff} = 4765\,K$, log g = 1.4, [Fe/H] = -2.35v$_{mic} = 1.6\,km/s$, based on color-effective temperature relations using broadband photometry measurements, Gaia satellite astrometric third data release DR3 data, and other existing relations.

3.2 Chemical Abundance Results

From equivalent width and the stellar parameters, and using the radiative transfer code MOOG [10] that converts line measurements into abundance values based on the physical conditions and absorption occurring in the star's outer layers (those are specified by the stellar parameters,) I obtained chemical abundances for each absorption line, log ϵ(X)_star, with X standing for all elements. For each element, I averaged these line abundances. Results are presented in Table 1. Some elements have only few line measurements, others have several dozen. Fe has about 200 lines measured.

From the log ϵ(X)_star measurements, I then calculated [X/H] values:

[X/H] = log ϵ(X)_star - log ϵ(X)_sun

using relevant values for the Sun (taken from the table in Figure 4), since this nomenclature of the bracket notation easily compares stellar values to that of the Sun.. A star with a lower, i.e. negative value, will have a subsolar value. A star with a higher abundance, i.e. a positive value, will have a supersolar value. Then, I calculated the final abundance, [X/Fe], in the following way:

[X/Fe] = [X/H] - [Fe/H]

Results are in Table 11. Abundances of light elements, iron-peak elements as well as some heavy elements were measured. In Figure 5, I compared the [X/Fe] abundances of J0449−5656 with known metal-poor stars from the literature [11]. As can be seen, the abundances all agree very well, which suggests that J0449−5656 is a typical halo star not unlike these other comparison stars.

3.3 Light element abundance trends

I measured lines of the following light elements: Li, Na, Mg, Si, Ca, Sc, Ti, and V. Abundances are listed in Table 11. As can be seem from Figure 5, J0449−5656 has an alpha-element enhancement of ∼0.4 dex (alpha-elements are Mg, Ca, and Ti), which is typical for stars that formed from gas enriched by a previous massive supernova explosion. This means the elements I observed in J0449−5656 were produced by this massive progenitor.

Element	$\log \epsilon$(X)	[X/H]	[X/Fe]	stdev	N
Li I	0.92	−0.13	2.22	0.25	1
Na I	4.10	−2.14	0.21	0.05	2
Mg I	5.49	−2.11	0.24	0.07	5
Si I	5.70	−1.81	0.54	0.15	2
Ca I	4.40	−1.94	0.41	0.27	23
Sc II	0.61	−2.54	−0.19	0.24	8
Ti I	2.56	−2.39	−0.04	0.16	15
Ti II	2.80	−2.15	0.20	0.18	27
V I	1.46	−2.47	−0.12	0.31	3
V II	1.88	−2.05	0.30	0.32	3
Cr I	3.10	−2.54	−0.19	0.29	12
Cr II	3.51	−2.13	0.22	0.36	3
Mn I	2.98	−2.45	−0.10	0.30	8
Fe I	5.15	−2.35	0.00	0.22	199
Fe II	5.18	−2.32	0.03	0.26	12
Co I	2.78	−2.21	0.14	0.18	5
Ni I	3.80	−2.42	−0.07	0.16	13
Zn I	2.26	−2.30	0.05	0.25	1
Sr II	0.83	−2.04	0.31	0.25	1
Ba II	0.05	−2.13	0.22	0.40	5
Eu II	0.13	−0.39	1.06	0.41	3

Table 1: Chemical abundances of J0449−5656.

3.4 Iron-peak abundance trends

I measured lines of the following iron-peak elements: Cr, Mn, Fe, Co, Ni, and Zn. Trends of iron-peak elements are often subsolar, ie. they have [X/Fe]<0. The abundance of J0449−5656 are all around 0, which is typical for metal-poor stars. These elements were also produced in the earlier supernova during explosive nucleosynthesis during the explosion.

3.5 Heavy element abundance trends

I measured lines of the following heavy elements: Sr, Ba, and Eu. These elements are made during other processes, such as the rapid (r-) neutron-capture process. I am finding enhancements in these elements, especially Eu, which suggests that J0449−5656 also has the signature of the r-process. This means that before J0449−5656 was born, another event made the heavy elements, such as a neutron-star-merger where these elements are synthesized in the early universe.

3.6 Abundance uncertainties

Together with the average abundance for each element, I also calculated the standard deviations of the mean. Standard deviation describes the width of the distribution of measurements. It also accurately reflects and describes the quality of the spectrum. Typical standard deviations are 0.1 to 0.35 dex, which is typical of the data quality of the original spectrum.

4 Nucleosynthetic Interpretation of Stellar Abundances

We also used the automated program Starfit (http://starfit.org/) to fit the abundance pattern of J0449−5656 with models from massive stars that exploded as supernovae in the early universe. Figure 6 shows the results. It is suggested that the massive progenitor had a mass of approximately 20 solar masses and a high explosion energy of 1.8 Bethe, which corresponds to 1.8 x 10^{52} ergs. This is called a hypernova. Hypernova are typically

	Elem.	Photosphere	Meteorites		Elem.	Photosphere	Meteorites
1	H	12.00	8.22 ± 0.04	44	Ru	1.75 ± 0.08	1.76 ± 0.03
2	He	$[10.93 \pm 0.01]$	1.29	45	Rh	0.91 ± 0.10	1.06 ± 0.04
3	Li	1.05 ± 0.10	3.26 ± 0.05	46	Pd	1.57 ± 0.10	1.65 ± 0.02
4	Be	1.38 ± 0.09	1.30 ± 0.03	47	Ag	0.94 ± 0.10	1.20 ± 0.02
5	B	2.70 ± 0.20	2.79 ± 0.04	48	Cd		1.71 ± 0.03
6	C	8.43 ± 0.05	7.39 ± 0.04	49	In	0.80 ± 0.20	0.76 ± 0.03
7	N	7.83 ± 0.05	6.26 ± 0.06	50	Sn	2.04 ± 0.10	2.07 ± 0.06
8	O	8.69 ± 0.05	8.40 ± 0.04	51	Sb		1.01 ± 0.06
9	F	4.56 ± 0.30	4.42 ± 0.06	52	Te		2.18 ± 0.03
10	Ne	$[7.93 \pm 0.10]$	-1.12	53	I		1.55 ± 0.08
11	Na	6.24 ± 0.04	6.27 ± 0.02	54	Xe	$[2.24 \pm 0.06]$	-1.95
12	Mg	7.60 ± 0.04	7.53 ± 0.01	55	Cs		1.08 ± 0.02
13	Al	6.45 ± 0.03	6.43 ± 0.01	56	Ba	2.18 ± 0.09	2.18 ± 0.03
14	Si	7.51 ± 0.03	7.51 ± 0.01	57	La	1.10 ± 0.04	1.17 ± 0.02
15	P	5.41 ± 0.03	5.43 ± 0.04	58	Ce	1.58 ± 0.04	1.58 ± 0.02
16	S	7.12 ± 0.03	7.15 ± 0.02	59	Pr	0.72 ± 0.04	0.76 ± 0.03
17	Cl	5.50 ± 0.30	5.23 ± 0.06	60	Nd	1.42 ± 0.04	1.45 ± 0.02
18	Ar	$[6.40 \pm 0.13]$	-0.50	62	Sm	0.96 ± 0.04	0.94 ± 0.02
19	K	5.03 ± 0.09	5.08 ± 0.02	63	Eu	0.52 ± 0.04	0.51 ± 0.02
20	Ca	6.34 ± 0.04	6.29 ± 0.02	64	Gd	1.07 ± 0.04	1.05 ± 0.02
21	Sc	3.15 ± 0.04	3.05 ± 0.02	65	Tb	0.30 ± 0.10	0.32 ± 0.03
22	Ti	4.95 ± 0.05	4.91 ± 0.03	66	Dy	1.10 ± 0.04	1.13 ± 0.02
23	V	3.93 ± 0.08	3.96 ± 0.02	67	Ho	0.48 ± 0.11	0.47 ± 0.03
24	Cr	5.64 ± 0.04	5.64 ± 0.01	68	Er	0.92 ± 0.05	0.92 ± 0.02
25	Mn	5.43 ± 0.05	5.48 ± 0.01	69	Tm	0.10 ± 0.04	0.12 ± 0.03
26	Fe	7.50 ± 0.04	7.45 ± 0.01	70	Yb	0.84 ± 0.11	0.92 ± 0.02
27	Co	4.99 ± 0.07	4.87 ± 0.01	71	Lu	0.10 ± 0.09	0.09 ± 0.02
28	Ni	6.22 ± 0.04	6.20 ± 0.01	72	Hf	0.85 ± 0.04	0.71 ± 0.02
29	Cu	4.19 ± 0.04	4.25 ± 0.04	73	Ta		-0.12 ± 0.04
30	Zn	4.56 ± 0.05	4.63 ± 0.04	74	W	0.85 ± 0.12	0.65 ± 0.04
31	Ga	3.04 ± 0.09	3.08 ± 0.02	75	Re		0.26 ± 0.04
32	Ge	3.65 ± 0.10	3.58 ± 0.04	76	Os	1.40 ± 0.08	1.35 ± 0.03
33	As		2.30 ± 0.04	77	Ir	1.38 ± 0.07	1.32 ± 0.02
34	Se		3.34 ± 0.03	78	Pt		1.62 ± 0.03
35	Br		2.54 ± 0.06	79	Au	0.92 ± 0.10	0.80 ± 0.04
36	Kr	$[3.25 \pm 0.06]$	-2.27	80	Hg		1.17 ± 0.08
37	Rb	2.52 ± 0.10	2.36 ± 0.03	81	Tl	0.90 ± 0.20	0.77 ± 0.03
38	Sr	2.87 ± 0.07	2.88 ± 0.03	82	Pb	1.75 ± 0.10	2.04 ± 0.03
39	Y	2.21 ± 0.05	2.17 ± 0.04	83	Bi		0.65 ± 0.04
40	Zr	2.58 ± 0.04	2.53 ± 0.04	90	Th	0.02 ± 0.10	0.06 ± 0.03
41	Nb	1.46 ± 0.04	1.41 ± 0.04	92	U		-0.54 ± 0.03
42	Mo	1.88 ± 0.08	1.94 ± 0.04				

Figure 4: The figure presents the element abundance in the present solar photosphere and the corresponding Cl carbonaceous chondrites values (Lodders, Palme & Gail 2009). From [1].

found to have enriched the gas from which metal-poor stars formed as they probably dominated the early universe.

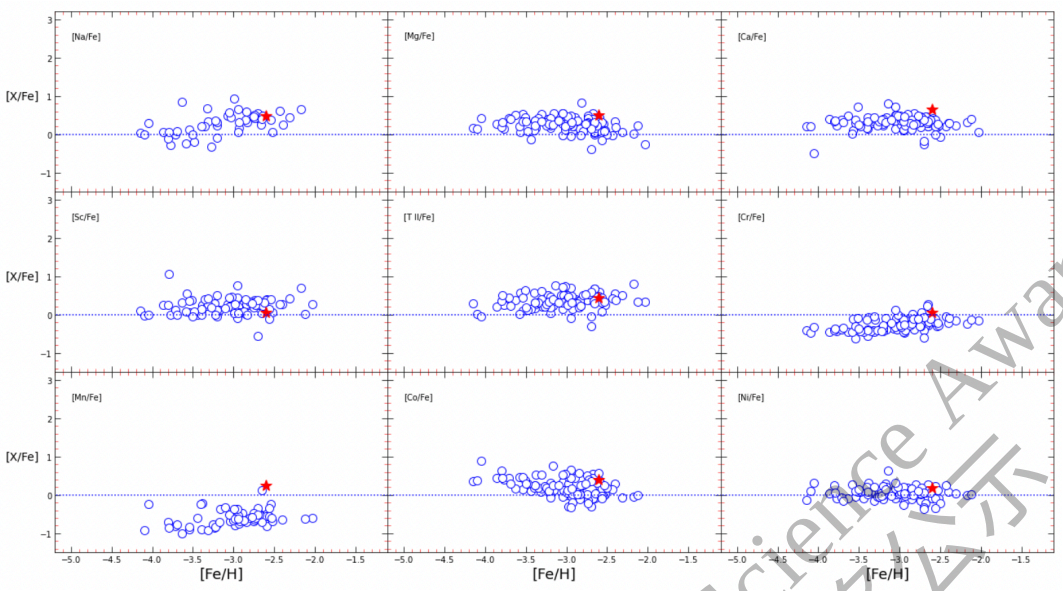

Figure 5: Comparison of selected abundances for J0449−5656 (red star) with literature metal-poor stars from [11] (blue circles).

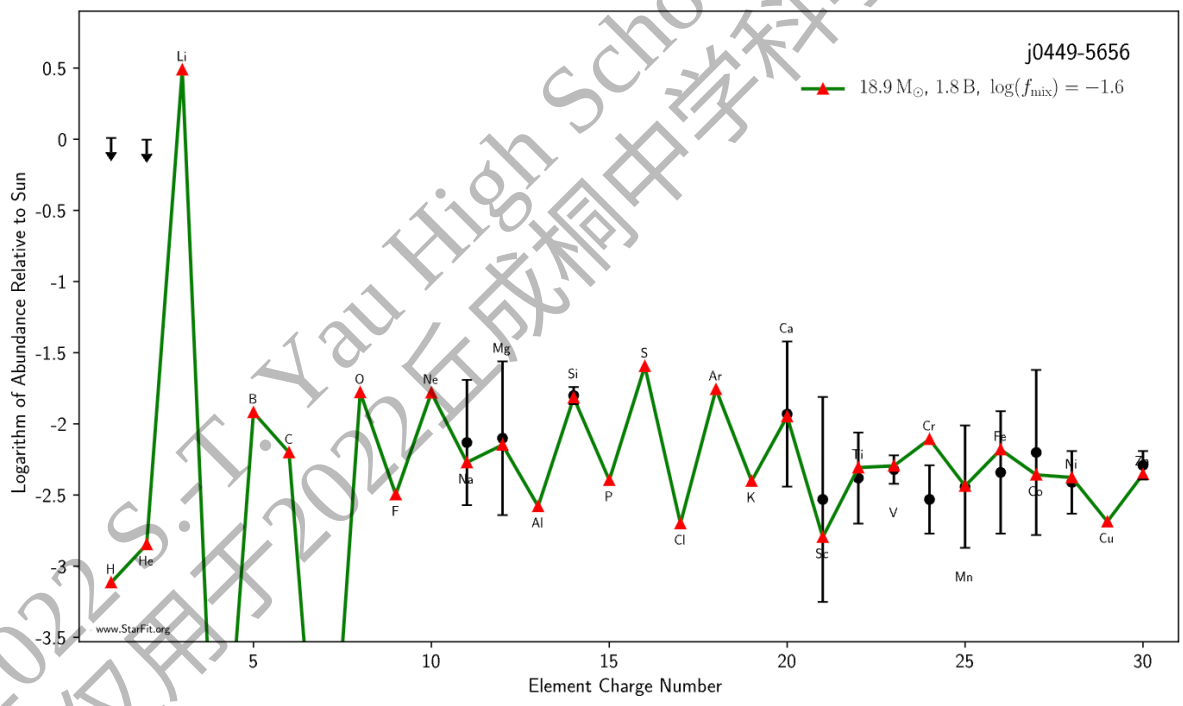

Figure 6: Results from a fitting of abundances with Starfit.

5 Kinematic Analysis

In the absence of the moon and heavy winter clouds in the nightsky, a band of light across the whole sky can be seen in any dark spot on Earth. This band of light is referred as the Milky Way in astronomy. The Milky Way is a gravitationally-bounded collection of stars which is often referred to simply as the "Galaxy." Galactic dynamics then studies the movement of celestial objects in the Galaxy. This leads to

Table 2: Gaia astrometry

Star	RA (α)	DEC (δ)	pmra (μ_α)	pmdec (μ_δ)	distance	RV
J0449−5656	38.1685	−37.1364	5.9374	−1.7505	10.9	246.1684

Table 3: Positions and Galactic Space-Velocity Components

Star	l	b	X	Y	Z	U	V	W
J0449−5656	244.4118	−66.4458	−1.6478	−3.4410	−8.7517	−159.1569	−318.4224	−113.3784

further studies of morphological and kinematical properties of our Galaxy. Therefore, linking the chemical abundances derived for my star J0449−5656 with its kinematic properties can provide information about its formation and evolution within the Milky Way.

5.1 Positions and Velocities

Positional astronomy, e.g. measuring position of stars in the sky, is called astrometry. It is the oldest branch of astronomy. However, this doesn't make astrometry old fashion or unimportant. Especially, recently, there have been major technological advances in obtaining astrometry measurements, e.g., with the Gaia satellite. The European Space Agency launched this satellite in 2013 (the Gaia satellite, [8]), with the aim to produce by far the most precise 3-D star map of our Galaxy.

Astronomers use the Gaia satellite to determine the location and motion of celestial bodies with unprecedented accuracy. The Gaia satellite is actually two telescopes that talk to three science instruments for making astronomical measurements of such quantities as position measurements, magnitudes (i.e. brightness), radial velocity, and basic chemical abundances.

A stellar orbit of any Galactic object can be determined from six parameters that describe its motion over time – right ascension R.A. (α), declination (δ), proper motion of R.A. (μ_α) and DEC (μ_δ), radial velocity, and distance. The R.A. and DEC can be found in the headers of the raw "fits" files provided by the telescope when the observation was taken. The remaining parameters can obtained from the Gaia Third Data Release (DR3, [8]), which I queried for these parameters (https://www.cosmos.esa.int/web/gaia/dr3). Table 2 lists all the required information for J0449−5656 to do a kinematic analysis.

The Gaia satellite is orbiting around the stable Langrange point L2 point of the Sun-Earth system (1.5 million km from the Earth in the anti-Sun direction). In addition, the Sun-Earth system is located 8 kpc from the center of the Milky Way. Therefore, I needed to transform the measurement obtained from Gaia into Galactocentric coordinates (X, Y, Z). Also, I needed to transform the proper motions ($\mu_\alpha \cos\delta$, μ_δ), and radial velocity measurements into rectangular Galactic velocities (U, V, W), using ready made programs that carried out most of the math. The Galactocentric positions and velocity can be calculated by applying a few orientation matrices provided by `Astropy` project `https://docs.astropy.org/en/stable/api/astropy.coordinates.Galactocentric.html`). This frame requires other inputs: the Sun-Galactic center distance, the height of the Sun above the Galactic midplane (it is not in the middle), and the velocity of the Sun in the Galactocentric frame as Cartesian velocity components. Table 3 lists the calculated Galactic positions and Galactic velocities.

5.2 Stellar Orbit Parameters and Origin of J0449−5656

After using programs to convert to the Galactocentric frame it is possible to backwards-integrate the stellar orbit of J0449−5656 to learn its history, using another very detailed program. To do so, I used `Galpy` which is a python package for Galactic dynamics. `Galpy` supports orbit integration in a given Galactic potential (`MWpotential2014`, [3]) for some specified amount of cosmic time. Once `Galpy` finished the stellar orbit integration, I accessed various orbital parameters for the star (e.g., orbital eccentricity, Zmax). For J0449−5656, I performed the orbital integration for the past 10 Gyr (i.e., backward stellar orbit integration).

Table 4 lists these calculated dynamical parameters for J0449−5656. The radial distance (R) is the distance from the z-axis (assumed to start at the center of the Galaxy) to the point of the star's projection on the x-y plane. The pericentric radius (r_{peri}) is the shortest distance between J0449−5656 and the center

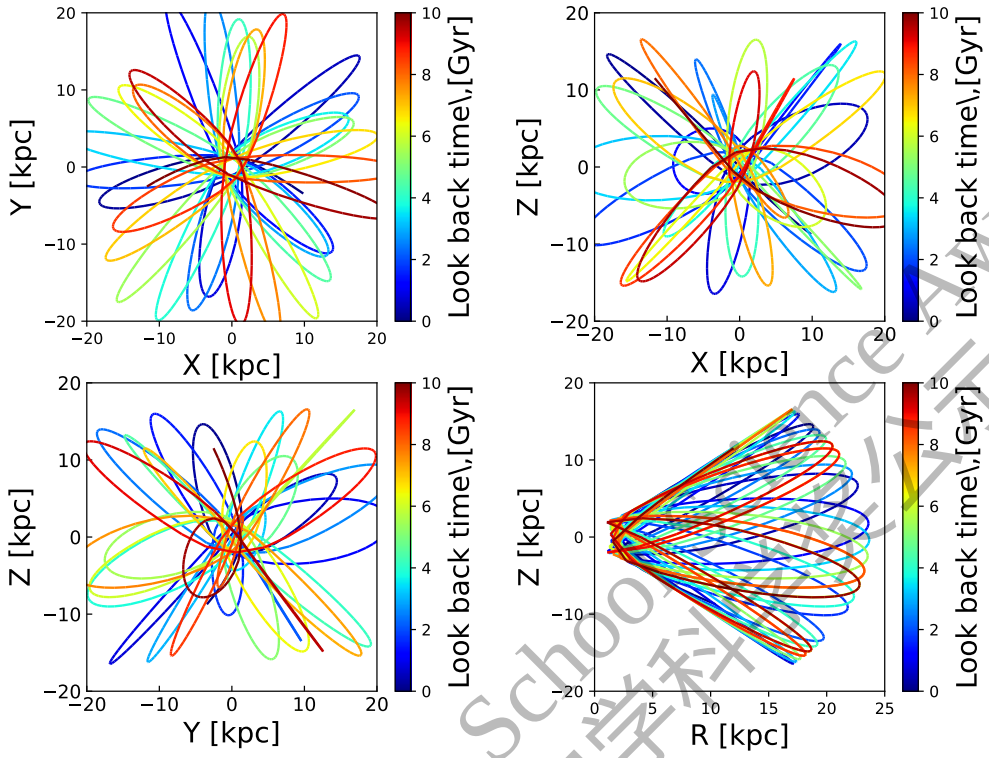

Figure 7: Projections of the J0449−5656 orbits in the X-Y (the upper left), X-Z (the upper right), Y-Z (the lower left), and R-Z (lower right). The orbit of J0449−5656 is eliptic and can reach a distance of 16 kpc above and below the Galactic plane. This unique orbit suggest that J0449−5656 resides at the Galactic halo.

of the Galaxy. The apocentric radius (r_{apo}) is the location of the greatest distance between J0449−5656 and the center of the Galaxy. These later two quantities can be used to calculate the orbital eccentricity as $e = (r_{apo} - r_{peri})/(r_{apo} + r_{peri})$, which is the elongation of J0449−5656's orbit. An eccentricity of e=0 is a circular orbit while e=1 is a very elliptical orbit. Finally, Z_{max} is the greatest distance that J0449−5656 could travel vertically (up or down) with respect to the Galactic x-y plane. This tells much about its history and origin.

Figure 7 shows the projections of the long-term (10 Gyr) orbital evolution of J0449−5656 in various Galactic planes. This shows that we can infer that J0449−5656 has an elliptic orbit with a maximum distance of $r_{apo} \approx 23$ kpc from the center of the Galaxy, and $Z_{max} \approx 16$ kpc from the Galactic x-y plane. The orbital parameters derived with the program indicate that J0449−5656 spend most of his age in the Galactic halo ($r_{apo} \approx 10$ kpc and $Z_{max} \approx 5$ kpc). This suggests that J0449−5656 most likely is a relic of an ancient fully disrupted dwarf galaxy that merged with the early Milky Way a long time ago.

Table 4: Orbital parameters of J0449−5656

Star	R [kpc]	r_{peri} [kpc]	r_{apo} [kpc]	z_{max} [kpc]	Eccentricity
J0449−5656	10.4	1.46	23.6	16.4	0.88

6 Summary and Conclusions

In this work, I studied a metal-poor star, J0449−5656, for its chemical abundances and kinematic properties. The goal was to learn about its origin and history.

The chemical abundance signature determined from many elements showed that the star has a typical pattern similar to that of other metal-poor stars located in the galactic halo. Lighter elements showed the typical alpha-enhancements. The heavy elements are enhanced, which suggests that J0449−5656 is a rare r-process metal-poor star that shows the chemical fingerprint of this rare nucleosynthesis process. Altogether this suggests that J0449−5656 formed from one of the earliest gas clouds in the universe that was enriched by at least two events: a massive 20 solar mass energetic hypernova and a neutron-star-merger, which provided the lighter and the heavy elements to the gas, respectively.

My kinematic analysis confirms my abundance results, which shows clearly that J0449−5656 is a halo star. For example because of its high z_{max} value of 16 kcp, which bring the star out into the halo for much of its time when its distance from the Galactic Center is not that much further than the Sun, with about 10 kpc.

Since J0449−5656 is undoubtedly a halo star, it was likely formed not in the Milky Way but in a small early dwarf galaxy that itself got accreted by the Milky Way many billions of years ago. This means that J0449−5656 is a cosmic immigrant that has resided in the Galaxy's outskirts, i.e. the halo, for some time. My findings about the massive progenitor star of J0449−5656 suggests that there were very early massive low-Fe stars in these early dwarf galaxies and that the first elements heavier than H and He were likely created in such small systems like the home system of J0449−5656.

References

[1] Martin Asplund et al. "The Chemical Composition of the Sun". In: 47.1 (Sept. 2009), pp. 481–522. DOI: 10.1146/annurev.astro.46.060407.145222. arXiv: 0909.0948 [astro-ph.SR].

[2] R. Bernstein et al. "MIKE: A Double Echelle Spectrograph for the Magellan Telescopes at Las Campanas Observatory". In: *Society of Photo-Optical Instrumentation Engineers (SPIE) Conference Series*. Ed. by M. Iye and A. F. M. Moorwood. Vol. 4841. Mar. 2003, p. 1694. DOI: 10.1117/12.461502.

[3] J. Bovy. "galpy: A python Library for Galactic Dynamics". In: 216, 29 (Feb. 2015), p. 29. DOI: 10.1088/0067-0049/216/2/29. arXiv: 1412.3451.

[4] A. Frebel. "Stellar archaeology: Exploring the Universe with metal-poor stars (Ludwig Biermann Award Lecture 2009)". In: *Astronomische Nachrichten* 331 (May 2010), pp. 474–488. DOI: 10.1002/asna.201011362.

[5] A. Frebel and J. E. Norris. "Near-Field Cosmology with Extremely Metal-Poor Stars". In: 53 (Aug. 2015), pp. 631–688. DOI: 10.1146/annurev-astro-082214-122423. arXiv: 1501.06921 [astro-ph.SR].

[6] Anna Frebel. *Searching for the oldest stars: Ancient relics from the early universe*. Princeton University Press, 2014.

[7] Anna Frebel et al. "Nucleosynthetic signatures of the first stars". In: 434.7035 (Apr. 2005), pp. 871–873. DOI: 10.1038/nature03455. arXiv: astro-ph/0503021 [astro-ph].

[8] Gaia Collaboration. "Gaia Data Release 3. Summary of the content and survey properties". In: *Astronomy and Astrophysics* (2022). DOI: 10.1051/0004-6361/202243940.

[9] Vinicius M. Placco et al. "Hubble Space Telescope Near-ultraviolet Spectroscopy of the Bright CEMP-no Star BD+44°493". In: 790.1, 34 (July 2014), p. 34. DOI: 10.1088/0004-637X/790/1/34. arXiv: 1406.0538 [astro-ph.SR].

[10] C. A. Sneden. "Carbon and Nitrogen Abundances in Metal-Poor Stars." PhD thesis. The University of Texas at Austin, 1973.

[11] D. Yong et al. "The Most Metal-Poor Stars. II. Chemical Abundances of 190 Metal-Poor Stars Including 10 New Stars With [Fe/H] -3.5". In: *ApJ* 762, 26 (Jan. 2013), p. 26. DOI: 10.1088/0004-637X/762/1/26. arXiv: 1208.3003 [astro-ph.GA].

Acknowledgements

Most importantly, I would like to sincerely thank my research supervisor Prof. Frebel from the Massachusetts Institute of Technology for her support and patience during the research process and writing of this paper, and all the information and guidance on the basic background theories relevant to this topic that she provided in order for me to complete this study. I would also like to thank Mohammad Mardini for his support during the research on the kinematics and dynamics of my star.

Appendix

Equivalent width measurements are listed in the following Tables 5 to 11. Note: "element" is given with one digit which indicates neutral (.0) or ionized species (0.1). "exit. pot." stands for excitation potential.

λ [Å]	element	exit. pot. [eV]	loggf [dex]	EW [mÅ]	$\log \epsilon$(X) [dex]
6707.80	3.0	0.00	0.17	21.7	0.92
5889.95	11.0	0.00	0.11	187.3	4.16
5895.92	11.0	0.00	−0.19	160.1	4.09
4057.51	12.0	4.35	−0.90	45.4	5.46
4167.27	12.0	4.35	−0.74	53.7	5.43
4702.99	12.0	4.33	−0.44	88.3	5.61
5172.68	12.0	2.71	−0.36	219.3	5.46
5183.60	12.0	2.72	−0.17	256.4	5.50
3905.52	14.0	1.91	−1.04	258.3	5.59
4102.94	14.0	1.91	−3.34	85.8	5.81
4318.65	20.0	1.90	−0.21	60.7	4.08
4425.44	20.0	1.88	−0.41	60.9	4.24
4454.78	20.0	1.90	0.26	79.5	4.00
4455.89	20.0	1.90	−0.55	54.2	4.25
4456.61	20.0	1.90	−1.74	13.8	4.52
4526.94	20.0	2.71	−0.47	11.2	4.06
4578.55	20.0	2.52	−0.67	16.6	4.24
4685.27	20.0	2.93	−1.02	11.4	4.85
5512.98	20.0	2.93	−0.45	32.4	4.83
5581.97	20.0	2.52	−0.58	29.6	4.42
5588.76	20.0	2.52	0.30	66.9	4.26
5590.12	20.0	2.52	−0.60	27.7	4.39
5601.29	20.0	2.53	−0.57	26.1	4.34
6102.72	20.0	1.88	−0.81	49.4	4.24
6122.22	20.0	1.89	−0.33	78.9	4.31
6162.17	20.0	1.90	−0.11	95.6	4.43
6166.44	20.0	2.52	−1.22	19.1	4.77
6169.06	20.0	2.52	−0.87	29.0	4.66
6169.56	20.0	2.53	−0.60	26.8	4.35
6439.07	20.0	2.52	0.33	70.1	4.23
6471.66	20.0	2.53	−0.71	46.8	4.85
6499.65	20.0	2.52	−0.81	11.4	4.07
6717.69	20.0	2.71	−0.58	36.9	4.73
4324.98	21.1	0.59	−0.44	65.6	0.35
4374.45	21.1	0.62	−0.42	80.2	0.70
4400.39	21.1	0.60	−0.54	51.7	0.16
4415.54	21.1	0.59	−0.67	72.0	0.70
4670.41	21.1	1.36	−0.58	34.2	0.74
5031.01	21.1	1.36	−0.40	55.7	0.91
5526.79	21.1	1.77	0.02	38.5	0.62
5657.91	21.1	1.51	−0.60	24.9	0.64
3989.76	22.0	0.02	−0.13	58.7	2.37
3998.64	22.0	0.05	0.02	73.8	2.64
4512.73	22.0	0.84	−0.40	18.4	2.62
4534.78	22.0	0.84	0.35	55.4	2.66
4548.76	22.0	0.83	−0.28	24.4	2.64
4555.48	22.0	0.85	−0.40	12.8	2.43
4656.47	22.0	0.00	−1.28	21.0	2.55
4681.91	22.0	0.05	−1.01	29.8	2.54
4840.87	22.0	0.90	−0.43	15.9	2.60
4981.73	22.0	0.84	0.57	68.2	2.63
4991.07	22.0	0.84	0.45	34.8	2.09

Table 5: Equivalent width measurements of J0449−5656.

λ [Å]	element	exit.	pot. [eV]	loggf [dex]	EW [mÅ]	$\log \epsilon$(X) [dex]
5016.16	22.0		0.85	−0.48	17.9	2.64
5173.74	22.0		0.00	−1.06	32.7	2.54
5192.97	22.0		0.02	−0.95	47.2	2.72
5210.38	22.0		0.05	−0.82	47.6	2.63
4028.34	22.1		1.89	−0.92	69.2	2.99
4337.91	22.1		1.08	−0.96	100.2	2.77
4394.06	22.1		1.22	−1.77	68.6	2.90
4395.84	22.1		1.24	−1.93	50.8	2.70
4398.29	22.1		1.21	−2.65	39.2	3.15
4399.77	22.1		1.24	−1.20	72.5	2.44
4417.71	22.1		1.17	−1.19	89.1	2.76
4418.33	22.1		1.24	−1.99	52.9	2.79
4443.80	22.1		1.08	−0.71	111.3	2.78
4444.55	22.1		1.12	−2.20	48.0	2.76
4450.48	22.1		1.08	−1.52	70.0	2.49
4464.45	22.1		1.16	−1.81	64.4	2.74
4470.85	22.1		1.17	−2.02	49.3	2.66
4493.52	22.1		1.08	−2.78	20.6	2.70
4533.96	22.1		1.24	−0.53	134.1	3.37
4571.97	22.1		1.57	−0.31	105.5	2.76
4583.41	22.1		1.16	−2.84	19.8	2.82
4636.32	22.1		1.16	−3.02	12.6	2.76
4657.20	22.1		1.24	−2.29	37.1	2.74
4708.66	22.1		1.24	−2.35	45.5	2.96
4798.53	22.1		1.08	−2.66	29.8	2.76
5129.16	22.1		1.89	−1.34	51.4	2.79
5185.90	22.1		1.89	−1.41	45.7	2.75
5188.69	22.1		1.58	−1.05	90.9	2.95
5336.79	22.1		1.58	−1.60	53.0	2.68
5381.02	22.1		1.57	−1.97	40.0	2.80
5418.77	22.1		1.58	−2.13	23.5	2.62
4111.78	23.0		0.30	0.40	26.4	1.44
4379.23	23.0		0.30	0.58	24.0	1.15
4389.98	23.0		0.28	0.22	37.1	1.77
3997.11	23.1		1.48	−1.20	25.0	1.68
4002.93	23.1		1.43	−1.44	42.6	2.25
4023.38	23.1		1.80	−0.61	36.4	1.71
4274.80	24.0		0.00	−0.22	128.0	3.38
4289.72	24.0		0.00	−0.37	130.0	3.56
4545.95	24.0		0.94	−1.37	21.2	2.97
4646.15	24.0		1.03	−0.74	24.6	2.52
4651.28	24.0		0.98	−1.46	23.3	3.15
4789.34	24.0		2.54	−0.33	14.0	3.55
5206.04	24.0		0.94	0.02	92.7	3.03
5296.69	24.0		0.98	−1.36	20.5	2.91
5298.28	24.0		0.98	−1.14	37.0	3.05
5345.80	24.0		1.00	−0.95	46.4	3.06
5348.31	24.0		1.00	−1.21	32.7	3.06
5409.77	24.0		1.03	−0.67	51.4	2.91
4558.64	24.1		4.07	−0.43	64.2	3.92
4588.20	24.1		4.07	−0.65	26.1	3.28
4618.81	24.1		4.07	−0.89	18.6	3.32

Table 6: Equivalent width measurements of J0449−5656.

λ [Å]	element	exit.	pot. [eV]	loggf [dex]	EW [mÅ]	$\log \epsilon$(X) [dex]
4030.75	25.0		0.00	−0.50	134.1	3.25
4033.06	25.0		0.00	−0.65	127.6	3.25
4034.48	25.0		0.00	−0.84	120.0	3.26
4041.35	25.0		2.11	0.28	57.1	2.87
4754.04	25.0		2.28	−0.08	26.3	2.63
4762.37	25.0		2.89	0.30	16.7	2.71
4823.52	25.0		2.32	0.14	32.5	2.59
6021.82	25.0		3.08	−0.05	18.2	3.24
4005.24	26.0		1.56	−0.58	121.0	4.99
4058.22	26.0		3.21	−1.18	37.5	5.37
4063.59	26.0		1.56	0.06	175.1	5.05
4067.98	26.0		3.21	−0.53	55.4	5.11
4070.77	26.0		3.24	−0.87	40.0	5.14
4071.74	26.0		1.61	−0.01	127.8	4.57
4114.44	26.0		2.83	−1.30	40.0	5.09
4132.06	26.0		1.61	−0.68	115.0	4.94
4134.68	26.0		2.83	−0.65	73.0	5.23
4143.87	26.0		1.56	−0.51	132.0	5.04
4147.67	26.0		1.49	−2.07	74.9	5.09
4150.25	26.0		3.43	−1.19	14.9	5.04
4154.50	26.0		2.83	−0.69	76.3	5.37
4156.80	26.0		2.83	−0.81	76.0	5.47
4157.78	26.0		3.42	−0.40	45.0	4.97
4158.79	26.0		3.43	−0.70	38.0	5.13
4174.91	26.0		0.91	−2.94	90.4	5.70
4175.64	26.0		2.85	−0.83	70.2	5.34
4181.76	26.0		2.83	−0.37	67.1	4.77
4182.38	26.0		3.02	−1.18	27.4	4.90
4184.89	26.0		2.83	−0.87	61.3	5.13
4187.04	26.0		2.45	−0.56	89.8	5.09
4187.80	26.0		2.42	−0.51	100.0	5.26
4191.43	26.0		2.47	−0.67	85.0	5.10
4195.33	26.0		3.33	−0.49	62.5	5.36
4199.10	26.0		3.05	0.16	85.4	5.02
4202.03	26.0		1.49	−0.69	120.0	4.89
4216.18	26.0		0.00	−3.36	101.1	5.30
4217.55	26.0		3.43	−0.48	47.4	5.11
4222.21	26.0		2.45	−0.91	79.9	5.17
4227.43	26.0		3.33	0.27	97.4	5.57
4233.60	26.0		2.48	−0.60	95.4	5.29
4238.81	26.0		3.40	−0.23	60.0	5.10
4250.12	26.0		2.47	−0.38	101.0	5.19
4250.79	26.0		1.56	−0.71	126.4	5.11
4260.47	26.0		2.40	0.08	115.0	4.95
4271.15	26.0		2.45	−0.34	110.0	5.31
4271.76	26.0		1.49	−0.17	150.0	4.85
4282.40	26.0		2.18	−0.78	96.0	5.21

Table 7: Equivalent width measurements of J0449−5656.

λ [Å]	element	exit.	pot. [eV]	loggf [dex]	EW [mÅ]	$\log \epsilon$(X) [dex]
4325.76	26.0		1.61	0.01	150.0	4.81
4352.73	26.0		2.22	−1.29	56.4	4.66
4375.93	26.0		0.00	−3.00	112.6	5.19
4388.41	26.0		3.60	−0.68	28.0	5.05
4404.75	26.0		1.56	−0.15	150.0	4.85
4415.12	26.0		1.61	−0.62	134.9	5.14
4427.31	26.0		0.05	−2.92	115.8	5.24
4430.61	26.0		2.22	−1.73	67.1	5.31
4432.57	26.0		3.57	−1.58	11.2	5.40
4442.34	26.0		2.20	−1.23	87.3	5.27
4443.19	26.0		2.86	−1.04	45.6	4.92
4447.72	26.0		2.22	−1.36	77.6	5.19
4461.65	26.0		0.09	−3.19	104.8	5.21
4466.55	26.0		2.83	−0.60	82.2	5.32
4484.22	26.0		3.60	−0.64	32.2	5.10
4489.74	26.0		0.12	−3.90	77.9	5.21
4494.56	26.0		2.20	−1.14	71.7	4.79
4514.18	26.0		3.05	−1.96	35.2	5.84
4531.15	26.0		1.48	−2.10	84.1	5.21
4547.85	26.0		3.55	−0.82	24.2	5.03
4592.65	26.0		1.56	−2.46	71.8	5.33
4595.36	26.0		3.30	−1.76	13.9	5.37
4602.00	26.0		1.61	−3.13	24.8	5.06
4602.94	26.0		1.49	−2.21	88.5	5.45
4607.65	26.0		3.27	−1.33	16.8	5.00
4619.29	26.0		3.60	−1.06	14.8	5.04
4630.12	26.0		2.28	−2.58	19.8	5.18
4637.50	26.0		3.28	−1.29	17.6	4.99
4643.46	26.0		3.65	−1.15	11.2	5.04
4647.43	26.0		2.95	−1.35	30.1	4.98
4661.97	26.0		2.99	−2.50	5.4	5.28
4668.13	26.0		3.27	−1.08	34.5	5.18
4704.95	26.0		3.69	−1.32	12.8	5.32
4733.59	26.0		1.49	−2.99	46.2	5.20
4736.77	26.0		3.21	−0.67	52.2	5.05
4789.65	26.0		3.55	−0.96	12.2	4.77
4871.32	26.0		2.87	−0.34	87.0	5.08
4872.14	26.0		2.88	−0.57	75.4	5.04
4875.88	26.0		3.33	−1.90	12.2	5.45
4882.14	26.0		3.42	−1.48	10.0	5.03
4890.76	26.0		2.88	−0.38	89.1	5.17
4891.49	26.0		2.85	−0.11	95.7	5.02
4903.31	26.0		2.88	−0.89	67.3	5.17
4907.73	26.0		3.43	−1.70	13.1	5.40
4910.02	26.0		3.40	−1.28	15.0	5.01
4918.99	26.0		2.86	−0.34	86.1	5.03
4920.50	26.0		2.83	0.07	95.0	4.79
4924.77	26.0		2.28	−2.11	44.3	5.20
4938.81	26.0		2.88	−1.08	53.2	5.06
4939.69	26.0		0.86	−3.25	58.0	4.91
4946.39	26.0		3.37	−1.11	22.9	5.03
4950.11	26.0		3.42	−1.50	13.0	5.17
4966.09	26.0		3.33	−0.79	31.8	4.87
4994.13	26.0		0.92	−2.97	77.6	5.12

Table 8: Equivalent width measurements of J0449−5656.

λ [Å]	element	exit.	pot. [eV]	loggf [dex]	EW [mÅ]	$\log \epsilon$(X) [dex]
5001.86	26.0		3.88	−0.01	42.9	4.96
5002.79	26.0		3.40	−1.46	16.6	5.23
5005.71	26.0		3.88	−0.12	37.9	4.97
5006.12	26.0		2.83	−0.62	36.2	4.20
5014.94	26.0		3.94	−0.18	35.9	5.05
5022.24	26.0		3.98	−0.33	24.0	4.98
5044.21	26.0		2.85	−2.02	15.7	5.12
5049.82	26.0		2.28	−1.36	76.2	5.11
5051.63	26.0		0.92	−2.76	93.9	5.29
5068.77	26.0		2.94	−1.04	53.8	5.08
5079.22	26.0		2.20	−2.10	61.7	5.42
5079.74	26.0		0.99	−3.24	73.2	5.35
5083.34	26.0		0.96	−2.84	83.8	5.16
5123.72	26.0		1.01	−3.06	78.0	5.30
5127.36	26.0		0.92	−3.25	75.3	5.32
5131.47	26.0		2.22	−2.52	34.3	5.32
5133.69	26.0		4.18	0.36	53.6	5.14
5141.74	26.0		2.42	−2.24	28.1	5.15
5150.84	26.0		0.99	−3.04	50.9	4.68
5151.91	26.0		1.01	−3.32	59.6	5.15
5166.28	26.0		0.00	−4.12	93.6	5.47
5191.45	26.0		3.04	−0.55	77.9	5.21
5192.34	26.0		3.00	−0.42	82.0	5.12
5194.94	26.0		1.56	−2.02	87.4	5.14
5198.71	26.0		2.22	−2.09	44.4	5.08
5202.34	26.0		2.18	−1.87	69.9	5.32
5215.18	26.0		3.27	−0.86	38.8	4.99
5216.27	26.0		1.61	−2.08	91.8	5.37
5217.39	26.0		3.21	−1.07	29.8	4.94
5225.53	26.0		0.11	−4.76	41.6	5.15
5232.94	26.0		2.94	−0.06	101.1	5.12
5242.49	26.0		3.63	−0.83	24.6	5.08
5253.46	26.0		3.28	−1.58	23.5	5.39
5263.31	26.0		3.27	−0.87	23.4	4.66
5266.56	26.0		3.00	−0.38	90.0	5.26
5281.79	26.0		3.04	−0.83	57.1	5.04
5283.62	26.0		3.24	−0.45	64.4	5.04
5307.36	26.0		1.61	−2.91	50.9	5.29
5322.04	26.0		2.28	−2.80	16.5	5.23
5324.18	26.0		3.21	−0.11	98.0	5.40
5332.90	26.0		1.56	−2.78	51.8	5.11
5339.93	26.0		3.27	−0.63	54.2	5.05
5341.02	26.0		1.61	−1.95	92.4	5.23
5364.87	26.0		4.45	0.23	34.0	5.17
5367.47	26.0		4.42	0.44	37.8	5.00
5369.96	26.0		4.37	0.54	35.7	4.81
5371.49	26.0		0.96	−1.64	141.3	5.24
5379.57	26.0		3.69	−1.42	17.7	5.54
5383.37	26.0		4.31	0.64	45.9	4.84
5397.13	26.0		0.92	−1.98	125.4	5.17
5405.77	26.0		0.99	−1.85	125.1	5.13
5410.91	26.0		4.47	0.40	44.0	5.22

Table 9: Equivalent width measurements of J0449−5656.

λ [Å]	element	exit.	pot. [eV]	loggf [dex]	EW [mÅ]	$\log \epsilon$(X) [dex]
5415.20	26.0		4.39	0.64	48.3	4.98
5429.70	26.0		0.96	−1.88	104.1	4.61
5434.52	26.0		1.01	−2.13	116.7	5.22
5483.10	26.0		4.15	−1.39	7.1	5.58
5497.52	26.0		1.01	−2.82	82.7	5.09
5501.47	26.0		0.96	−3.05	70.5	5.00
5506.78	26.0		0.99	−2.79	88.5	5.16
5554.90	26.0		4.55	−0.27	10.9	5.12
5569.62	26.0		3.42	−0.52	60.8	5.22
5586.76	26.0		3.37	−0.11	72.5	5.00
5624.54	26.0		3.42	−0.76	36.6	4.99
5638.26	26.0		4.22	−0.72	16.3	5.39
5662.52	26.0		4.18	−0.41	26.8	5.32
5686.53	26.0		4.55	−0.44	18.7	5.57
5701.54	26.0		2.56	−2.14	21.3	5.01
5753.12	26.0		4.26	−0.62	17.8	5.38
5816.37	26.0		4.55	−0.60	5.3	5.10
6056.00	26.0		4.73	−0.32	21.4	5.72
6065.48	26.0		2.61	−1.41	50.3	4.91
6136.61	26.0		2.45	−1.41	72.7	5.14
6137.69	26.0		2.59	−1.35	69.1	5.18
6173.34	26.0		2.22	−2.88	16.3	5.17
6191.56	26.0		2.43	−1.42	66.3	4.99
6213.43	26.0		2.22	−2.48	16.7	4.78
6219.28	26.0		2.20	−2.45	35.8	5.17
6230.72	26.0		2.56	−1.28	71.9	5.11
6232.64	26.0		3.65	−1.24	11.7	5.05
6240.65	26.0		2.22	−3.17	7.9	5.09
6246.32	26.0		3.60	−0.77	27.2	4.98
6252.56	26.0		2.40	−1.77	59.4	5.17
6265.13	26.0		2.18	−2.54	29.6	5.11
6297.79	26.0		2.22	−2.64	50.5	5.65
6301.50	26.0		3.65	−0.71	49.9	5.43
6322.69	26.0		2.59	−2.47	21.2	5.33
6336.82	26.0		3.69	−0.85	37.7	5.38
6344.15	26.0		2.43	−2.88	15.2	5.37
6355.03	26.0		2.84	−2.29	20.3	5.42
6393.60	26.0		2.43	−1.58	64.8	5.11
6408.02	26.0		3.69	−0.99	20.4	5.13
6411.65	26.0		3.65	−0.59	34.9	5.01
6421.35	26.0		2.28	−2.01	51.8	5.11
6430.85	26.0		2.18	−1.95	62.2	5.12
6494.98	26.0		2.40	−1.24	94.1	5.32
6592.91	26.0		2.73	−1.47	48.2	5.03
6593.87	26.0		2.43	−2.37	26.3	5.15
6609.11	26.0		2.56	−2.66	14.6	5.27
6677.99	26.0		2.69	−1.42	60.3	5.15
6750.15	26.0		2.42	−2.58	34.1	5.50
6843.66	26.0		4.55	−0.73	6.4	5.27
6855.16	26.0		4.56	−0.49	19.7	5.61
6978.85	26.0		2.48	−2.45	17.7	5.04
7495.07	26.0		4.22	−0.10	29.2	5.02
7511.02	26.0		4.18	0.12	76.3	5.67

Table 10: Equivalent width measurements of J0449−5656.

λ [Å]	element	exit.	pot. [eV]	loggf [dex]	EW [mÅ]	$\log \epsilon$(X) [dex]
7568.90	26.0		4.28	−0.88	15.8	5.52
4178.86	26.1		2.58	−2.51	55.8	4.95
4233.16	26.1		2.58	−2.02	70.8	4.80
4303.17	26.1		2.70	−2.52	82.7	5.73
4416.82	26.1		2.78	−2.57	55.3	5.18
4491.41	26.1		2.86	−2.71	38.4	5.05
4508.28	26.1		2.86	−2.42	60.8	5.22
4515.34	26.1		2.84	−2.60	65.2	5.48
4583.83	26.1		2.81	−1.94	82.2	5.18
4620.52	26.1		2.83	−3.21	14.9	4.91
5197.58	26.1		3.23	−2.22	50.7	5.15
5234.63	26.1		3.22	−2.18	50.7	5.11
5325.55	26.1		3.22	−3.16	18.2	5.36
3842.05	27.0		0.92	−0.74	60.2	2.67
3845.47	27.0		0.92	0.06	84.4	2.57
3995.31	27.0		0.92	−0.18	83.2	2.69
4118.77	27.0		1.05	−0.48	79.9	2.99
4121.32	27.0		0.92	−0.33	88.1	2.93
4604.99	28.0		3.48	−0.24	14.3	3.77
4648.65	28.0		3.42	−0.09	14.1	3.54
4686.22	28.0		3.60	−0.59	4.6	3.70
4714.42	28.0		3.38	0.25	35.3	3.69
4756.52	28.0		3.48	−0.27	9.7	3.59
4904.41	28.0		3.54	−0.17	17.4	3.85
4980.17	28.0		3.60	0.07	24.1	3.86
5080.53	28.0		3.65	0.32	29.9	3.79
5081.11	28.0		3.85	0.30	27.9	4.00
5084.08	28.0		3.68	0.03	17.2	3.79
5115.40	28.0		3.83	−0.11	17.4	4.11
5476.90	28.0		1.83	−0.78	87.3	3.91
6643.63	28.0		1.68	−2.22	23.1	3.73
4810.54	30.0		4.08	−0.15	24.8	2.25
4077.71	38.1		0.00	0.15	233.0	0.83
4554.03	56.1		0.00	0.14	157.4	0.33
4934.08	56.1		0.00	−0.16	163.6	0.59
5853.68	56.1		0.60	−0.91	49.2	−0.38
6141.71	56.1		0.70	−0.03	95.4	−0.21
6496.90	56.1		0.60	−0.41	92.4	−0.07
4129.72	63.1		0.00	0.22	83.4	−0.34
4205.04	63.1		0.00	0.21	104.4	0.31
4435.58	63.1		0.21	−0.11	93.8	0.41

Table 11: Equivalent width measurements of J0449−5656.